Available online at www.sciencedirect.com

SCIENCE DIRECT®

Physics of the Earth and Planetary Interiors 153 (2005) 181–190

PHYSICS OF THE EARTH AND PLANETARY INTERIORS

www.elsevier.com/locate/pepi

Experimental evaluation of magnetic interaction in pyrrhotite bearing samples

F. Wehland[a,c,*], A. Stancu[b,1], P. Rochette[c,2], M.J. Dekkers[d,3], E. Appel[a,4]

[a] *Institut für Geowissenschaften, Abteilung Geophysik, Universität Tübingen, Sigwartstr. 10, 72076 Tübingen, Germany*
[b] *Faculty of Physics, 'Alexandru Ioan Cuza' University, Blvd. Carol I, 11, 700506, Iaşi, Romania*
[c] *C.E.R.E.G.E, (UMR CNRS—Université, d'Aix-Marseille III), Europôle Méditerranéen de l'Arbois, BP 80, Aix en Provence cedex 04, France*
[d] *Paleomagnetic Laboratory 'Fort Hoofddijk', Faculty of Earth Sciences, Utrecht University, Budapestlaan 17, 3584 CD Utrecht, The Netherlands*

Received 12 February 2004; received in revised form 21 December 2004; accepted 2 May 2005

Abstract

Pyrrhotite bearing metamorphic limestones have recently experienced an increasing relevance in paleomagnetic research. Simple univectorial remanences document the metamorphic uplift, whereas more complex multicomponent pTRMs may constrain its age. For a successful application of the latter, it is important to estimate the degree of magnetic interactions to ensure the additivity of individual pTRM segments. We therefore have subjected the sized dispersed suite (<5–250 μm) of TTE pyrrhotite to FORC analysis and compared the result with remanence-based parameters like the ΔM or the irreversible susceptibility. This is used as a basis to evaluate the response of marly limestone samples from regionally metamorphic areas (Bourg d'Oisans, France) and contact-metamorphic aureoles (Elba, Italy; Skye, Scottland; Manaslu area, Nepal) to these techniques. The results show that the techniques are able to estimate the nature and – to a certain degree – the intensity of the magnetic interaction. The different dominant magnetic states of the assemblage can also be unravelled as well. Based on the remanence measurements of the TTE samples, a relationship between grain-size and the irreversible susceptibility is established in order to estimate the mean grain-size fraction in natural particle distribution.

Keywords: Magnetic interaction; ΔM analysis; Irreversible susceptibility; FORC analysis; Pyrrhotite

1. Introduction

Secondary pyrrhotite is formed in low-grade metamorphic limestones at the expense of pyrite and magnetite within the 200–450 °C temperature range (Lambert, 1973; Rochette, 1987; Schill et al., 2002). The need to investigate magnetic interactions in pyrrhotite bearing metamorphic limestones arose from the use of such rocks as a recorder of Earth's Magnetic Field Reversals (Rochette et al., 1992; Crouzet et al., 1999, 2001a,b). Independent partial thermoremanent magnetization (pTRM), i.e. identical blocking and unblock-

* Corresponding author. Present address: Shell International EP B.V., Kessler Park 1, Postbus 60, 2288 GS Rijswijk, The Netherlands. Tel.: +49 7071 2974698; fax: +49 7071 295842.

E-mail addresses: florian.wehland@uni-tuebingen.de (F. Wehland), ALSTANCU@UAIC.RO (A. Stancu), rochette@cerege.fr (P. Rochette), dekkers@geo.uu.nl (M.J. Dekkers), erwin.appel@uni-tuebingen.de (E. Appel).

[1] Tel.: +40 232 201175; fax: +40 232 201205.

[2] Tel.: +33 4 42 97 15 62; fax: 33 4 42 97 15 40.

[3] Tel.: 31 30 253 1671; fax: 31 30 243 1677.

[4] Tel.: 49 7071 2974132; fax: 49 7071 295842.

0031-9201/$ – see front matter
doi:10.1016/j.pepi.2005.05.006

ing spectra, are mandatory for such studies. Therefore, the samples should consist of a non-interacting single domain (SD)-particle assemblage (Thellier and Thellier, 1959). The tendency to crystallize mainly below the single domain threshold (∼<2 μm; Soffel, 1977) favours the use of pyrrhotite as a pTRM recorder. Nevertheless, clustering of pyrrhotite grains, the presence of multidomain (MD) particles, or an incomplete metamorphic reaction can cause magnetic interaction during pTRM recording processes.

In the past, experimental investigation of magnetic interaction was hampered by the lack of fast and reliable experimental methods. For natural magnetite, Dunlop (1972) concluded that ratios of M_{rs}/M_s (saturation remanence/saturation magnetization) of 0.5 and higher are characteristic of non-interacting SD grains. This was supported by Davis and Evans (1976), who showed that this ratio can be lowered due to interaction. Cisoswski (1981) used a plot of IRM_r versus a.f.-demagnetised SIRM (acquisition of isothermal remanent magnetisation versus alternating field demagnetised saturation IRM), where non-interacting grains exhibit symmetrical curves. Other methods to examine magnetic interaction like the off-diagonal Preisach diagram for SD particle interaction (Daniel and Levine, 1960; Woodward and Della Torre, 1960) or the inverse anhysteretic susceptibility (Kneller, 1969; Veitch, 1990 were later on questioned by Dunlop et al. (1990). New input came from studies of magnetic recording media (Spratt et al., 1988; Fearon et al., 1990; Mayo et al., 1990, Mayo et al., 1991a,b) where mostly remanence measurements were used to study magnetic interaction. Petrovský et al. (1993) tried to transfer these ideas to natural systems concluding that, despite some promising results, more extensive studies are necessary to decisively delineate texture, concentration, and type of the magnetic carriers as function of the differential remanence behaviour. Nevertheless, the remanence-based methods are useful to detect the degree and general character of magnetic interaction. The recently developed first order reversal curves (FORC) diagram (Pike et al., 1999; Roberts et al., 2000) seems to be an appropriate technique to obtain information about switching fields and interactions in magnetic particle systems. For this study we applied the remanence-based methods as well as the FORC method on artificial and natural pyrrhotite bearing samples.

2. Theory

The problem of measuring magnetic interaction by a remanence-based technique was first discussed by Wohlfarth (1958) who concluded that for a non-interacting uniaxial SD particle assemblage the relationship of the different normalized remanence acquisitions can be described by:

$$M_{dc}(H) = 1 - 2M_r(H), \tag{1}$$

where M_r and M_{dc} are the normalized isothermal remanences (IRMs) acquired from the a.f.-demagnetized state and during dc backfield demagnetization of the SIRM, respectively. For MD particles this relationship is not valid due to self-demagnetization effects.

By plotting M_r versus M_{dc} (Henkel, 1964) the ideal case of non-interacting uniaxial SD-particles will lead to a straight line with a slope of −2. In 1990, Mayo et al. introduced the deviation from this line expressed by the differential remanence parameter (Speliotis and Lynch, 1991) $\Delta M(H)$, a formulation that has been used since then:

$$\Delta M(H) = M_{dc}(H) - (1 - 2M_r(H)). \tag{2}$$

For a SD particles assemblage the resulting deviation is ascribed to many-body effects and generally indicates the presence of magnetic inter-particle interaction (Fearon et al., 1990; Mayo et al., 1991a,b). Positive values of ΔM are interpreted as a result of positive interaction, which tends to stabilize the magnetization, whereas a negative value would come from negative interaction yielding a net demagnetising effect (see Petrovský et al., 1993). Nevertheless, one has to take into account that results from MD particles can be congruent with results from SD particles. Important for successful experiments is the perfect alignment of the samples in both directions during IRM acquisition and backfield IRM. A small deviation can have a significant influence on the results, normally tending to negative ΔM at lower coercivities.

The differential susceptibility of the remanence χ_r and χ_{dc} can be calculated from M_r and M_{dc} curves (IRM curves) as the first derivative d(M)/dH. The ratios of χ_r and χ_{dc} (here introduced as W parameter) should follow the Wohlfarth equation giving a value of two for a non-interacting case. The spectra of χ_r and χ_{dc} are quantified by the position of the maxima and the shape parameter full-width-at-half-maximum (FWHM). It is important here to note the dependence of IRM curves and related parameters on the initial magnetization state (Fearon et al., 1990; Heslop et al., 2004). It is conventional to start from a three axial static a.f.-demagnetized state as it is the most reproducible one (Stancu et al., 2001, and references therein).

The FORC diagram is calculated from a set of partial hysteresis curves (see Mayergoyz, 1986). The measurement of a FORC starts with the saturation of the sample in a high positive field. The field is afterwards decreased to the reversed field H_a, and the FORC is the magnetization curve measured from H_a back to saturation. A set of FORCs is obtained by repeating this measurement for different values of H_a. At the applied field H_b on a FORC starting from H_a the magnetization is denoted as $M(H_a, H_b)$, where $H_b > H_a$. The FORC distribution $\rho(H_a, H_b)$ is then defined as the mixed second derivative:

$$\rho(H_a, H_b) = -\frac{1}{2}\frac{\partial^2 M(H_a, H_b)}{\partial H_a \partial H_b}, \quad (3)$$

where $\rho(H_a, H_b)$ is defined for $H_b > H_a$. It became convenient for plotting the FORC distribution to use the coordinate system $\{H_c = (H_b - H_a)/2, H_u = (H_a + H_b)/2\}$ instead of the original $\{H_a, H_b\}$. As $H_b > H_a$, $H_c > 0$, and the FORC diagram is plotted as a contour plot in the right-hand half plane with H_u and H_c as the vertical and horizontal axis, respectively. The H_c coordinate is referred to microcoercivity. Further details about the derivation of Eq. (3) and the change of the coordinates can be found in Pike et al. (1999, 2005).

Experimental results for monoclinic pyrrhotite gave a single domain threshold at around 1.5–2 μm (Soffel, 1977), a PSD range up to grains of 40 μm, and pure MD behaviour for grains larger 40 μm (Soffel, 1981). Dekkers (1989) also found a value for the SD threshold of 1–2 μm. Clark (1984) found a slightly higher value of about 3 μm for the single domain threshold.

3. Samples and methods

The size dispersed fractions of natural pyrrhotite from the Temperino in Tuscany, Italy (TTE samples) used in this study had already been subjected to different measurements in the past (Dekkers, 1988a,b; Dekkers, 1989; Worm et al., 1993). The material was available as 7 mm cylindrical samples with distinct grain-size factions of (μm): <5; 5–10; 10–15; 15–20; 20–25; 25–30; 30–40; 40–55; 55–75; 75–100; 100–150; and 150–250. Material for preparing the samples was selected from a pyrometasomatic pyrrhotite–pyrite–chalcopyrite ore zone at Temperino (Tuscany, Italy). The pyrrhotite fractions contain equidimensional grains. Magnetite is absent in these rocks and the presence of intergrowths is rare. Sample preparation was performed in an inert atmosphere to prevent alteration. The resulting grain-size fractions were checked using transmitted and reflected light microscopy and X-ray diffraction; the grain-size ranges were controlled optically. Monoclinic pyrrhotite has been proven as the dominant magnetic phase; only in the smallest fraction traces of hexagonal pyrrhotite were identified only in the smallest fraction. The grain-size fractions were homogeneously dispersed in an epoxy resin matrix with about 2% pyrrhotite by volume. For more details see Dekkers (1988a,b).

Natural samples were taken from contact-metamorphic limestones of the Isle of Skye, Scotland, the Manaslu area, Nepal (Schill et al., 2004) and Elba Island, Italy. Also, regional metamorphic limestones near Bourg d'Oisans, France (Crouzet et al., 1999) were selected for the present study. The samples were cut in cubes or cylinders with an edge length or diameter of 10 mm, respectively.

All samples were subjected to a.f.-demagnetization of 120 mT prior to any further treatment using an three axis static 2G600 a.f.-demagnetiser. A Micromag 3900 Vibrating Sample Magnetometer (lodged in CEREGE) carried out all magnetization and remanence experiments and measurements. Generally, FORC diagrams are based on a set of 100 individual FORCs with a smoothing factor (SF) of two, an average time of 0.25 s, zero waiting time and a saturation field of 700 mT. For weaker samples the average time was increased to 5 s on a set of not less than 80 FORCs. Due to smoothing not all values down to $H_c = 0$ can be plotted. For imparting high fields of 9 T a MMPM9 pulse magnetiser has been used.

4. Results and discussion

4.1. Sized dispersed fractions

FORC diagrams of all grain-size fractions are shown in Fig. 1. For the smaller grain-size fractions (<5 to 30–40 μm) the contours of the plot are generally closed indicating an SD to PSD behaviour. For the coarser fractions the open contour lines stand for their MD behaviour. With decreasing grain size the maximum of the distributions are shifted to higher coercivities with an increasing tendency to deviate from the horizontal line (Fig. 2). The deviation from the H_c-axis in combination with a negative slope of the line of contour elongation can be interpreted as a consequence of a positive mean interaction field (Roberts et al., 2000). The asymmetry in the diagrams with respect to the H_c-axis is most pronounced in the small grain-size fractions leading to sharp negative (white) regions in the lower half. These negative regions are always placed at higher coercivities than the peak and are decreasing with increasing grain-size. The negative regions become negligible for coarser grain-sizes (Fig. 1). Comparing the asymmetries in the FORC diagrams with those obtained by micromagnetic and phenomenological (Preisach-type) modelling of interacting ferromagnetic SD particles systems (Stancu et al., 2003) underlines the presence of positive mean interaction fields in these samples.

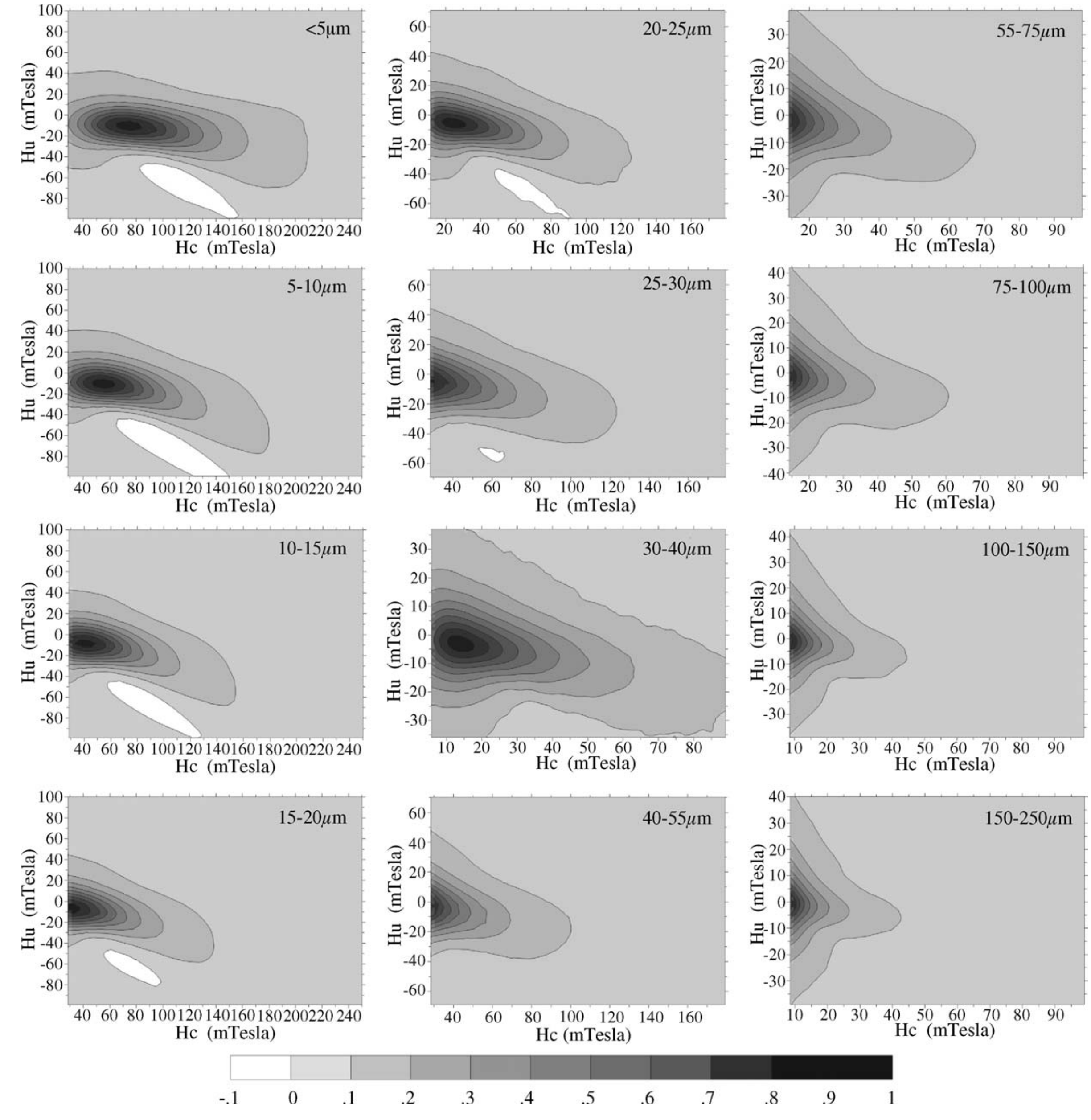

Fig. 1. FORC diagrams of all grain-size fractions from the TTE series (Dekkers, 1988a,b). The samples show a decreasing asymmetry regarding their horizontal axis and a vanishing of the negative area with increasing grain-size. Note that the coordinates are different for the sake of illustration.

The differential remanence parameter ΔM (Fig. 3) for the smaller grain-size fractions is positive at lower fields and decreases to a small negative value at fields higher 0.3 T. A pattern like this is characteristic for a system of SD particles with statistical as well as positive mean field interaction fields. The positive starting value of the curves (implying a local minimum at low coercivities) is a consequence of the incomplete a.f. demagnetisation; the remanence carried by the high coercive component was not affected (cf. Fig. 4). In general, lower coercivities are observed with increasing particle size. In the coarser grain-size fractions (40–55 μm and greater) the ΔMs are negative from the beginning with a minimum at low fields that is most pronounced in the coarsest fraction. The 30–40 μm set, marking the upper limit of the PSD range (Soffel, 1981), has an intermediate shape and is still positive at lower fields, but without a local minimum. The initial negative values can be linked to the

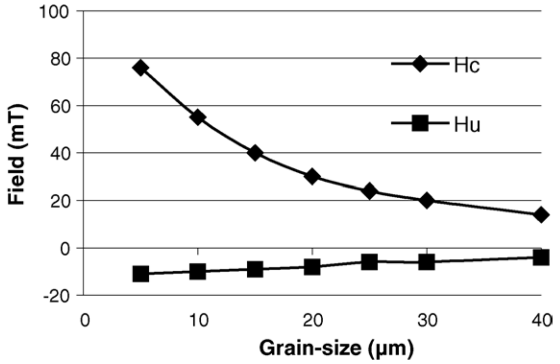

Fig. 2. Position of the distribution maxima in the FORC diagram. The coercivity (H_c) shows a decrease with increasing grain size. The deviation from the horizontal line (H_u) shows a more linear dependence.

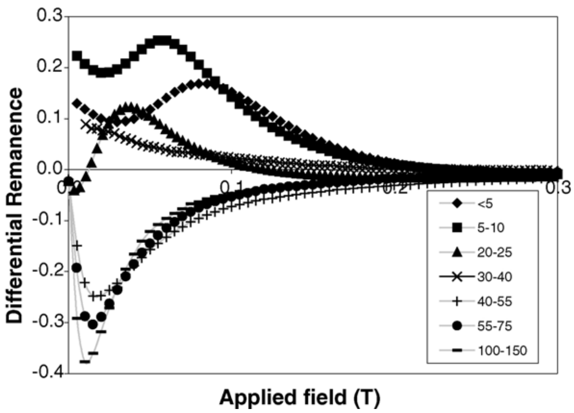

Fig. 3. Differential remanence parameter ΔM (see text for explanation) as a function of the applied field for selected grain-size fractions (µm). A clear change in the type of interaction can be seen at the 30–40 µm fraction (upper limit of the PSD range).

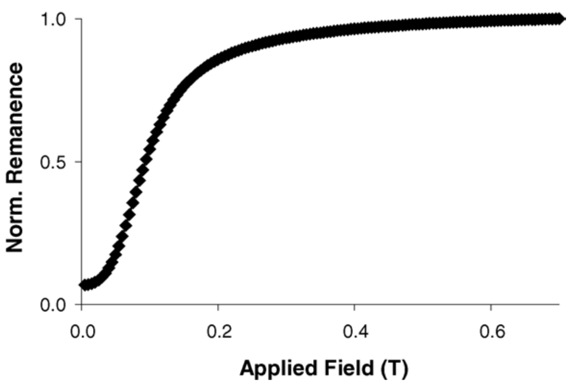

Fig. 4. Normalized IRM acquisition curve for the <5 µm fraction. The incomplete a.f. demagnetization causes a residual remanence at zero fields.

magnetization process related with domain wall motion and, therefore, is expected for MD samples.

The change in shape of the ΔM-plots between the 30–40 and 40–55 µm range, which may be interpreted as the transition from a dominant SD/PSD towards a dominant MD behaviour, is more pronounced than in the FORC diagrams, where a gradual opening of the individual contour lines marks the transition.

The appearance of a positive interaction field using the ΔM method is well pronounced in the smaller fractions and strongest in sample 5–10 µm. The lower M_s in the <5 µm fraction is in coincidence with Dekkers (1988b) and can be related to the continual existence of micro twins as a consequence of substantial hammering during sample preparation. Differences appear in the interaction pattern of the coarser samples, where in the FORC diagram – despite a dominant MD behaviour – the positive mean interaction field can still be detected.

The general trend mentioned above can be made clearer by the comparison of the peak position for χ_r and χ_{dc}. This occurs at higher fields for M_{dc} for the smaller fractions as a result of a stabilizing mean interaction field, and changes to lower fields for the coarser fractions due to the destabilizing mean interaction field as expected for multidomain particles (Fig. 5). The relationship of the intensities of the calculated susceptibility curves (Table 1) is less clear in this matter. After equation (2), $W = 2$ is expected for non-interacting SD particles. In our case, the values of the smaller fractions (up to 30–40 µm) are below two with a minimum in the 20–25 µm fraction. For the coarser fractions (40–50 µm

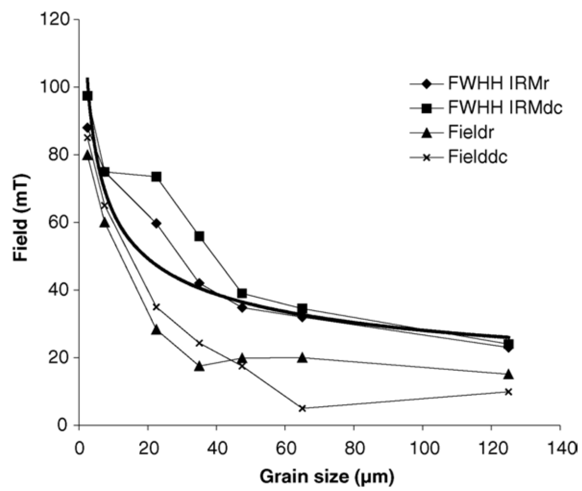

Fig. 5. FWHH and peak position ($\mathrm{Field_r}$ and $\mathrm{Field_{dc}}$) of the calculated differential susceptiblity. The thick black line is the exponentionally fitted trendline for the FWHH $\mathrm{IRM_r}$ curves.

Table 1
Parameters derived from the calculated susceptibility for selected samples

Sample	FWHM IRM_r	FWHM IRM_{dc}	$Field_r$	$Field_{dc}$	W	Eq. (4)	Eq. (5)	DS	M_{rs}/M_s	H_{cr}/H_c
TTE150	23.0	24.0	15.1	9.9	2.31	154.0	94.3	MD	0.24	0.89
TTE75	32.0	34.5	20.0	5.0	2.20	64.1	94.3	MD	0.26	1.01
TTE55	34.8	39.0	19.9	17.5	2.07	51.3	46.5	MD	0.29	0.89
TTE40	42.0	55.9	17.5	24.3	1.99	31.2	38.3	PSD	0.35	0.89
TTE25	59.7	73.5	28.3	35.0	1.73	12.3	18.5	PSD	0.36	0.74
TTE10	75.0	74.9	60.0	65.0	1.97	6.7	5.6	SD-PSD	0.44	0.96
TTE5	88.0	97.4	79.9	85.1	1.99	4.4	3.4	SD	0.47	0.97
E2	60	70	45	29.8	1.96	12.1	13.8	PSD	0.31	3.24
E3	61	70	60	40.1	1.97	11.6	8.3	PSD	0.26	2.66
S3	60	65	40	29.8	2.21	12.1	15.6	PSD	0.38	1.12
S2	115	103	60	35.0	2.34	2.2	9.1	SD	0.59	1.17
S5	62	63	25	15.0	2.27	11.1	41.4	PSD	0.39	1.45
M1	180	215	125	120.0	2.00	0.7	1.7	SD	0.66	1.53

$Field_r$ and $Field_{dc}$ denote the position of the calculated susceptibility peaks. The columns with Eqs. (4) and (5) give the calculated mean of the grain-size fraction after formula (4) and (5), respectively. DS stands for the interpreted dominating domain state in the assemblage. For FWHM and the W parameter see text. The rock magnetic parameters of M_{rs}/M_s and H_{cr}/H_c are added for the sake of completeness.

and higher) the ratio is greater than 2 due to the demagnetizing effect of the interaction field. In contrast, the FWHM parameter, which can be seen as a measure of the switching field distribution (SFD), is not influenced by stabilizing or demagnetizing interaction fields. The value and difference between the FWHM derived from χ_r and χ_{dc} decrease with increasing grain-size related only to a narrowing of the SFD.

Due to its direct correlation with the grain-size fractions and independence of the character of the mean interaction field, the FWHM can be used as a measure for the grain-size fraction in the natural systems. Derived from χ_r the relationship between FWHM (F) and mean value of the grain-size (S_{mean}) is expressed by:

$$S_{mean}\,(\mu m) = 629974F\,(mT)^{-2.6524} \tag{4}$$

with $R^2 = 0.9296$. The calculated values for the TTE samples are listed in Table 1. A function derived from χ_{dc} was abandoned due to the higher noise of the data. The influence of the character of the mean interaction fields on the position of the susceptibility peaks ($Field_r$ in Fig. 5) hampers the use of this parameter as an indicator for a mean grain-size. We tried to overcome this problem by taking a mean value (P_{mean}) of both peak positions from the IRM_r and IRM_{dc}. The resulting relationship is expressed as:

$$S_{mean}\,(\mu m) = 7902.7P_{mean}\,(mT)^{-1.7531} \tag{5}$$

with $R^2 = 0.9581$. An advantage in the use of the peak position is its independence of the shape of the particle distribution. As in the hypothetical case of grains with only one specific coercivity a FWHM derived function does not work, the peak position is still a direct measure of the grain-size. But in general, both for natural and artificial samples this case remains hypothetical.

The results from FORC diagrams and remanence measurements in terms of the domain state are in good agreement with observations described in the literature (Roberts et al., 2000; Pike et al., 1999; Stancu et al., 2001, 2003; Muxworthy and Dunlop, 2002; Carvallo et al., 2003). For both techniques, the SD to PSD transition is more gradual, whereas the change to the MD behaviour is quite pronounced as a consequence of the change in the mean field interaction fields during this transition. Experiments with high fields (9 T) imparted parallel or perpendicular to the applied field did not change the shape and dimension of the FORC distributions. This could mean that FORC diagrams for this kind of samples are not sensitive to the magnetic history of the sample.

4.2. Natural samples

One sample (M1) from the Manaslu area (Nepal) containing only pyrrhotite (proven by thermal demagnetisation of the IRM on a twin sample) was selected. The IRM acquisition curve of M1 is not entirely saturated in 0.7 T (Fig. 6) indicating a high coercive part of the pyrrhotite particle distribution. The derived ΔM parameter starts with low negative values changing to positive values at higher coercivities. The negative starting values are probably due to the residual remanence and the orientation problem in the magnetometer. With a maximal deviation from the Henkel plot of −0.086 magnetic interaction is nearly absent in this sample (Fig. 6). This is supported by $W = 2.00$. The calculated mean of the

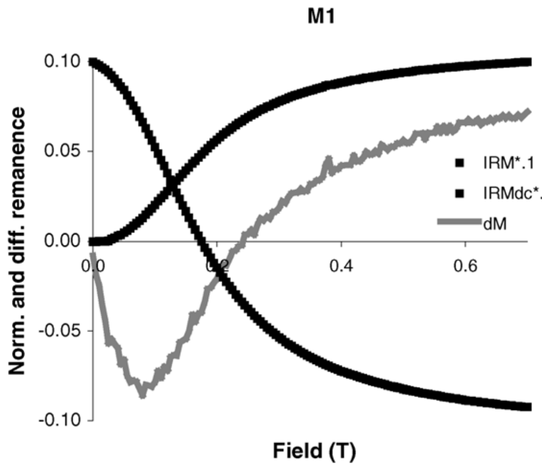

Fig. 6. IRM, IRM_{dc} and ΔM (grey) for the M1 sample. The IRM-values are reduced by 0.1 for a better illustration.

grain-size fraction after Eq. (4) is around 1 μm (Table 1) and points towards a clear SD behaviour.

In the FORC diagram (Fig. 7), the distribution is well elongated with a negligible vertical spread, closed contours and no obvious deviation from the horizontal line. This shape stands for a non-interacting SD particle system with a high coercivity peak of the distribution at $H_c = 125$ mT. The extension over the right border is due to the non-saturated parts in the particle system. The result from the FORC analysis coincides with the observation from the remanence measurements.

Similar FORC diagrams are obtained from samples of the western Alps (Fig. 8). For the representative sample $F9$ the shape of the distribution is an elongated one with a maximal coercivity of $H_c \sim 400$ mT. The contour lines are closed indicating SD behaviour of the assemblage. The enhanced vertical spread ($H_u = 20$ mT) is due to the higher smoothing factor (SF = 3). The FORC diagrams

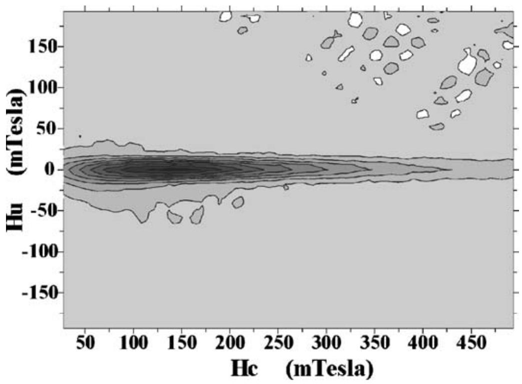

Fig. 7. FORC diagram of sample M1 (SF = 2, $t_{avr} = 0.25$ s, 100 FORCs). The distribution shows a clear SD particle assemblage. Interaction seems to be absent.

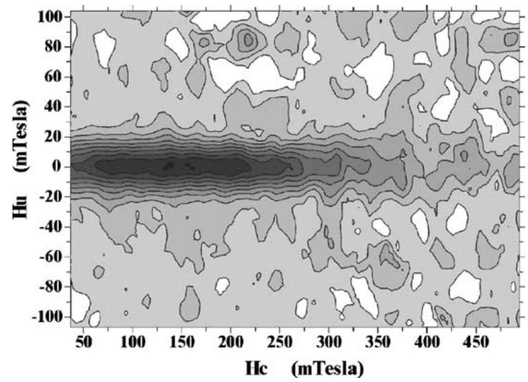

Fig. 8. FORC diagrams from samples of Bourg d'Oisans. The elongated and closed contours along H_c up to 400 mT standing for a pure SD particles distribution with high coercivities (picture with SF = 3 $t_{avr} = 5$ s, 80 FORCs).

indicate a broad SD particle assemblage and underline the good recording qualities for a pTRM record in samples taken at Bourg d'Oisans as shown by Crouzet et al. (1999).

In the Elba (E) samples the coercivity distribution along H_c as taken from the FORC diagrams (Fig. 9) have a maximal extent of 90 mT. The shape of the distribution is still elongated and the vertical spread with $H_u < 15$ mT indicates weak magnetic interactions. The differential remanence parameter exhibits a small negative interaction field ($\Delta M > -0.15$). Together with the other parameters derived from remanence and rockmagnetic measurements (Table 1) the samples fall into the PSD range.

For the samples of the Isle of Skye (S) thermal demagnetization of IRM discloses that the samples contain large (up to mm scale) pyrrhotite and magnetite. This was confirmed by reflected light microscopy and SEM, which reveal intergrowths of pyrrhotite with magnetite, pyrite and chalcopyrite. Consequently, the interaction patterns in the FORC diagrams of these samples are manifold (Fig. 10). Sample S3 comes closest to the results from the artificial samples (deviation from the H_c-axis, the negative tilt of the distribution, negative region in lower half of the diagram). In the upper half the contours are slightly bent to higher values of H_u. In sample S2, the counters are bent stronger in the upper half of the diagram. The negative region, the deviation and the tilt in the distribution are less pronounced. Additionally, the sample has a high coercive component up to 400 mT. The behaviour of this sample can be regarded as a transitional one between S3 and S5, where bent counters are in the upper and lower half and the negative region is absent. Together with a long tail indicating a high coercive component this pattern is termed "bird-structure",

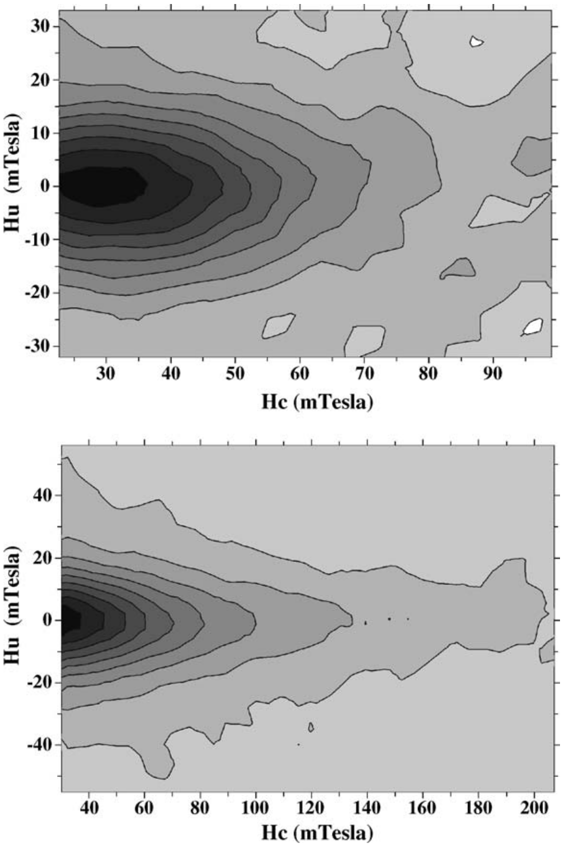

Fig. 9. FORC diagrams from samples from the Elba. The closed contours and the peak position around 30 mT indicates a dominantly PSD assemblage. Signs of mean interaction field are absent (both pictures with SF = 3).

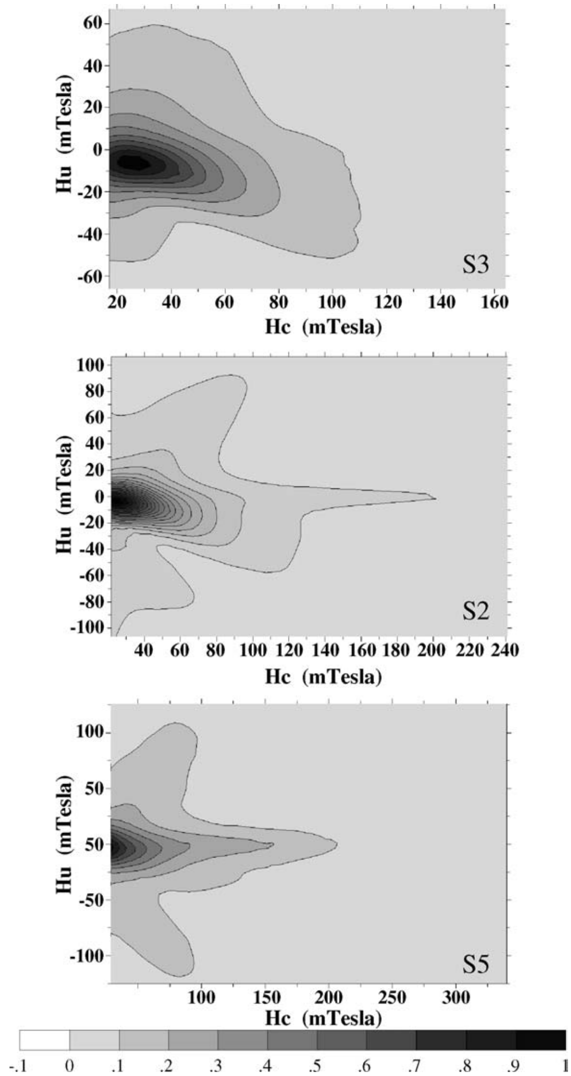

Fig. 10. FORC diagrams from samples from the Isle of Skye, where different magnetic phases (pyrrhotite, magnetite) are present.

where the bent areas are acting as the wings. In general, these features point towards a positive mean interaction field.

The differential remanence ΔM for S3 und S2 (<-0.18) stands for a highly negative mean interaction field, which is supported by $W > 2$. Due to the broader grain-size distribution the calculated mean of the grain-size distribution is at 3 μm for sample S2. On the contrary, the ΔM for sample S5 contains a local minimum and maximum, both low in amplitude and located at high fields (Fig. 11).

A tentative interpretation for S3 and the <40 μm TTE samples could be that both have a minor contribution of hexagonal pyrrhotite (not detected by other means) intergrown with the monoclinic phases in a sandwich like manner (one layer demagnetizes the other), whereas the patterns of S2 and S5 are the consequence of the magnetic interaction with other phases like magnetite. In addition, natural samples do of course obtain larger MD particles, which will lead to negative values of the

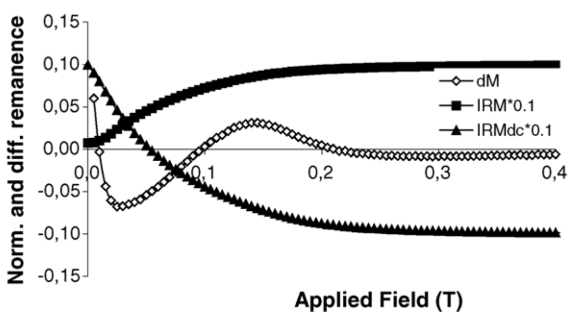

Fig. 11. IRM, IRM_{dc} and ΔM curves for sample S5. The intensities of the IRM curves and the *x*-axis were changed for illustration.

ΔM plot at lower coercivities. As the ΔM plot does not cover the entire coercivity spectra of pyrrhotite, nothing is known about the mean interaction fields from 0.4 T up to the full saturation of pyrrhotite.

These results clearly demonstrate the difficulties in comparing similar FORC measurements (especially: S3 and the respective size-dispersed fractions) with other methods like the ΔM plot. Once again, this could be due to the orientation problem of the sample in the magnetometer during IRM acquisition and backfield IRM and its influence on the ΔM plot (negative values at low coercivities).

In the light of recording successive, independent pTRMs in pyrrhotite, the absence of magnetic interaction and the dominance of SD particles in samples from the regional metamorphic setting of Bourg d'Oisans support the rockmagnetic results made by Rochette et al. (1992) and Crouzet et al. (1999, 2001a,b). The potential for TRM recording in contact metamorphic rocks as derived from the magnetic interaction analysis strongly depends on the different locations. In the Manaslu area, where clear non-interaction SD assemblages are found, a violation of the laws of independent pTRMs (Thellier and Thellier, 1959) will not be expected. Under such conditions, for the Elba samples the restricted coercivity spectrum and a major domain state between SD and PSD grains limit their use as a pTRM recorder. In such a case, their pTRM recording qualities should additionally be checked by pTRM experiments.

In the samples from the Isle of Skye the recording of independent pTRMs during cooling of the rock can be excluded due to their high magnetic interaction. The above observations support the use of magnetic interaction techniques as a pre-selective tool for Thellier like experiments as proposed by Wehland and coworkers (in press) for basaltic samples.

5. Conclusion

Both techniques used here, FORC and remanence based, are suitable to estimate the degree and nature of magnetic interaction in pyrrhotite bearing samples, although the ΔM plot is far more sensitive to the orientation of the sample during the experiment. The grain-size related change in the domain state is in good agreement with the literature and can be derived from FORC analysis as well as from the remanence and rock magnetic based techniques. The relationship between grain-size and SFD as derived from the artificial samples and expressed by FWHM-parameter can be described by a simple function, which helps to estimate the mean grain-size. Other parameters like the *W*-parameter, hysteresis parameters or the peak position of χ_r and χ_{dc} can enhance the understanding of the nature of the interaction field, grain-size distribution and domain state.

For natural systems we have shown that pyrrhotite can exist as an ideal non-interacting SD-particle assemblage in contact and regional metamorphic rocks. Nevertheless, intergrowths with other phases like magnetite or hexagonal pyrrhotite can often lead to high interaction fields of a different nature. This seems to be more likely in contact metamorphic rocks, where the process of pyrrhotite formation often leads to mixed assemblages and a less pronounced grain-size distribution. In the context of pTRM experiments secondary pyrrhotite has the potential as a good recorder if the degree of interaction is checked by one of the methods used above.

Acknowledgement

The authors would like to thank David Dunlop and Michael Jackson for their helpful comments made during the review of this paper. We acknowledge F. Vadeboin for her help in setting the VSM in CEREGE, and C. Pike and T. Mullender for letting us use their FORC programs. We also wish to thank Florence Heath for improving the readability of the paper. Financially, we would like to thank the Deutsche Forschungsgemeinschaft (DFG) for its support.

References

Carvallo, C., Muxworthy, A.R., Dunlop, D.J., Williams, W., 2003. Micromagnetic modelling of first-order reversal curves (FORC) diagrams for single-domain and pseudo-single domain magnetite. Earth Planet. Sci. Lett. 213, 375–390.

Cisoswski, S., 1981. Interacting vs. non-interacting single domain behaviour in natural and synthetic samples. Phys. Earth Planet. Int. 26, 56–62.

Clark, D.A., 1984. Hysteresis properties of sized dispersed monoclinic pyrrhotite grains. Geophys. Res. Lett. 11, 173–176.

Crouzet, C., Ménard, G., Rochette, P., 1999. High precision three dimensional paleothermometry derived from paleomagnetic data in an Alpine metamorphic unit. Geology 27 (6), 503–506.

Crouzet, C., Rochette, P., Ménard, G., 2001a. Experimental evaluation of thermal recording of polarity reversals during metasediments uplift. Geophys. J. Int. 145, 771–785.

Crouzet, C., Stang, H., Appel, E., Schill, E., Gautam, P., 2001b. Detailed analysis of successive pTRMs carried by pyrrhotite in Himalayan metacarbonates: an example from Hidden Valley. Central Nepal. Geophys. J. Int. 146, 607–618.

Daniel, E.D., Levine, I., 1960. Experimental and theoretical investigation of the magnetic properties of iron oxides recording tape. J. Acoust. Soc. Am. 32, 1–15.

Dekkers, M.J., 1988a. Some rockmagnetic parameters for natural goethite, pyrrhotite and fine-grained hematite. PhD thesis, University of Utrecht, Geologica Ultraiectina, 51, 231 pp.

Dekkers, M.J., 1988b. Magnetic properties of natural pyrrhotite. Part I. Behaviour of initial susceptibility and saturation-magnetization-related rock-magnetic parameters in a grain-size dependent framework. Phys. Earth Planet. Int. 52, 376–393.

Dekkers, M.J., 1989. Magnetic properties of natural goethite. I. Grain size dependence of some low- and high-field related rockmagnetic parameters measured at room temperature. Geophys. J. 97, 323–340.

Davis, P.M., Evans, M.E., 1976. Interacting single-domain properties of magnetic intergrowths. J. Geophys. Res. 81, 989–994.

Dunlop, D.J., 1972. Magnetite: behaviour near the single domain threshold. Science 176, 41–43.

Dunlop, D.J., Westcott-Lewis, M.F., Bailey, M., 1990. Preisach diagram and anhysteresis: do they measure interaction? Phys. Earth Planet. Int. 65, 62–77.

Fearon, M., Chantrell, R.W., Wohlfarth, E.P., 1990. A theoretical study of interaction effects on the remanence curves of particle dispersions. J. Magn. Magn. Mater. 86, 197–206.

Henkel, O., 1964. Remanenzverhalten und wechselwirkungen in hartmagnetischen teilchenkollektiven. Phys. Status Solidi (b) 161, K41–K44.

Heslop, D., McIntosh, G., Dekkers, M.J., 2004. Using time- and temperature-dependent Preisach models to investigate the limitations of modelling isothermal remanent magnetization acquisition curves with cumulative log Gaussian functions. Geophys. J. Int. 157, 55–63.

Kneller, E., 1969. Fine particle theory. In: Berkowitz, A.E., Kneller, E. (Eds.), Magnetism and Metallurgy, Vol. I. Academic Press, New York, pp. 365–471.

Lambert, I.B., 1973. Post-depositional availability of sulphur and metals and formation of secondary textures and structures in stratiform sedimentary sulphide deposits. J. Geol. Soc. Aust. 20, 205–215.

Mayergoyz, I.D., 1986. Mathematical model of hysteresis. IEEE Trans. Mag. MAG-22, 603–608.

Mayo, P.I., Erkkila, R.M., Bradbury, A., Chantrell, R.W., 1990. Interaction effects in longitudinally oriented and non-oriented barium hexaferrite tapes. IEEE Trans. Magn. MAG-26, 1894–1896.

Mayo, P.I., O'Grady, K., Chantrell, R.W., Cambridge, J.A., Sanders, I.L., Yogi, T., Howard, J.K., 1991a. Magnetic measurement of interaction effects in CoNiCr and CoPtCr thin film media. J. Mag. Mag. Mater. 95, 109–117.

Mayo, P.I., O'Grady, K., Kelly, P.E., Cambridge, J., Sanders, I.L., Yogi, T., Chantrell, R.W., 1991b. A magnetic evaluation of interaction and noise characteristics of CoNiCr thin films. J. Appl. Phys. 69 (8), 4733–4735.

Muxworthy, A.R., Dunlop, D.J., 2002. First-order reversal curve (FORC) diagrams for pseudo-single-domain magnetites at high temperature. Earth Planet. Sci. Lett. 203, 369–382.

Petrovský, E., Hejda, P., Zelinka, T., Kropáček, V., Šubrt, J., 1993. Experimental determination of magnetic interaction within a system of synthetic haematite particles. Phys. Earth Planet. Int. 76, 123–130.

Pike, C.R., Roberts, A.P., Verosub, K.L., 1999. Characterizing interactions in fine magnetic particle systems using first order reversal curves. J. Appl. Phys. 85, 6660.

Pike, C.R., Ross, C.A., Scalettar, R.T., Zimanyi, G., 2005. First-order reversal curve diagram analysis of a perpendicular nickel nanopillar array. Phy. Rev. B 71 (134407), 1–12.

Roberts, A.P., Pike, C.R., Verosub, K.L., 2000. First-order reversal curve diagrams: a new tool for characterizing the magnetic properties of natural samples. J. Geophys. Res. 105 (B12), 28461–28475.

Rochette, P., 1987. Metamorphic control of the magnetic mineralogy of black shales in the Swiss Alps: towards the use of "magnetic isograds". Earth Planet. Sci. Lett. 84, 446–456.

Rochette, P., Ménard, G., Dunn, R., 1992. Thermochronometry and cooling rates deduced from single sample records of successive magnetic polarities during uplift of metamorphic rocks in the Alps (France). Geophys. J. Int. 108, 491–501.

Schill, E., Appel, E., Gautam, P., 2002. Towards pyrrhotite/magnetite geothermometry in low-grade metamorphic carbonates of the Tethyan Himalaya (Shiar Khola, Central Nepal). J. Asian Earth Sci. 20, 195–201.

Schill, E., Appel, E., Crouzet, C., Gautam, P., Wehland, F., Staiger, M., 2004. Oroclinal bending versus regional significant clockwise rotations in the Himalayan arc—constraints from secondary pyrrhotite remanences. In: Sussman, A.J., Weil, A.B. (Eds.), Orogenic Curvature: Integrating Paleomagnetic and Structural Analyses. Geol. Soc. Am. Special Paper 383, 73–85.

Soffel, H., 1977. Pseudo single domain effects and single domain—multidomain transition in natural pyrrhotite deduced from domain structure observations. J. Geophys. 42, 351–359.

Soffel, H.C., 1981. Domain structure of natural fine-grained pyrrhotite in a rock matrix (diabase). Phys. Earth Planet. Int. 26, 98–106.

Speliotis, D.E., Lynch, W., 1991. Magnetic interaction in particulate and thin-film recording media. J. Appl. Phys. 69, 4496–4498.

Spratt, G.W.D., Bissel, P.R., Chantrell, R.W., 1988. Static and dynamic experimental studies of particulate recording media. J. Mag. Mag. Mater. 75, 309–318.

Stancu, A., Stoleriu, L., Cerchez, M., 2001. Micromagnetic interaction of statistical and mean-field interactions in particulate ferromagnetic media. J. Mag. Mag. Mater. 225, 411–417.

Stancu, A., Pike, C., Stoleriu, L., Postolache, P., Cimpoesu, D., 2003. Micromagnetic and Preisach analysis of the first order reversal curves (FORC) diagram. J. Appl. Phys. 93 (10), 6620–6622.

Thellier, E., Thellier, O., 1959. Sur l'intensité du champ magnétique terrestre dans le passé historique et géologique. Ann. Geophys. (15), 285–376.

Veitch, R.J., 1990. Anhysteretic susceptibility and static magnetic properties in interacting small particles. IEEE Trans. Magn. MAG-26, 1876–1878.

Wohlfarth, E.P., 1958. Relations between different modes of the acquisition of the remanent magnetization of ferromagnetic particles. J. Appl. Phys. 29, 595–596.

Woodward, J.G., Della Torre, E., 1960. Particle interaction in magnetic recording tapes. J. Appl. Phys. 31, 56–62.

Worm, H.U., Clark, D., Dekkers, M.J., 1993. Magnetic susceptibility of pyrrhotite: grain size, field and frequency dependence. Geophys. J. Int. 114, 127–137.